XLIII CILAMCE
21–25, November, 2022
FOZ DO IGUAÇU – PR – BRAZIL

A meshfree approach for geometrically exact shear-deformable beams

Felipe P. dos Santos[1], Enzo Marino[2], Lapo Gori[1]

[1]*Dept. of Structural Engineering, Federal University of Minas Gerais*
Avenida Antonio Carlos, 6627, 31270-901, Belo Horizonte/MG, Brazil
felipe-pereira@ufmg.br, lapo@dees.ufmg.br
[2]*Dept. of Civil and Environmental Engineering, University of Florence*
Via di Santa Marta, 3 - 50139 Firenze, Italy
enzo.marino@unifi.it

Abstract. Besides the finite element method (FEM), a number of numerical methods have been proposed in the literature for the analysis of geometrically exact shear deformable beams, developed to improve the convergence properties and the shear-locking behaviour exhibited by the finite element method. This paper illustrates some preliminary results obtained with the application of a meshfree method of the family of Smoothed Point Interpolation Methods (SPIMs) to the analysis of a geometrically exact shear deformable beam. Among the possibilities of shape functions creation, the so-called edge-based approach with polynomial basis is extended for this one-dimensional model. A classic example is solved numerically to validate the code. The resulting nonlinear system of equations is treated by a Newton-like algorithm with load control.

Keywords: Smoothed point interpolation methods (SPIMs), Edge-based, Geometrically exact beam

1 Introduction

The smoothed point interpolation methods are from a family of meshfree methods were the concepts of smoothing domains and weakened-weak W^2 formulation are introduced. Among the possibilities of domain tessellations in these methods, are the node-based smoothed point interpolation method (NS-PIM) proposed by Liu et al. [1], the cell-based smoothed point interpolation method (CS-PIM) introduced in the work of Zhang and Liu [2] and finally the edge-based smoothed point interpolation method (ES-PIM) addressed in Liu and Zhang [3]. A comprehensive discussion concerning to these methods can be found in Liu and Zhang [4]. The SPIMs emerged to solve two and three dimensional problems, however applications for one dimensional problems are also available in the literature, e.g. Liu [5], Du et al. [6], He et al. [7] and Santos et al. [8].

In this paper the ES-PIM will be investigated on the analysis of the geometrically exact beam model proposed by Simo [9] and Simo and Vu-Quoc [10]. The ES-PIM simulations were performed using the MATLAB® software. The code was validated and the numerical results were compared with the ones available in the relevant literature.

2 Geometrically exact beam

The geometrically exact model adopted in this paper is characterised by a three-dimensional motion, where displacements and rotations are allowed without any restriction in magnitude Simo [9], Simo and Vu-Quoc [10]. The beam is a three-dimensional object characterised by a family of cross sections and a line of centroids. In the *current configuration* the line of centroids $\varphi_0(S,t)$ is a curve defined on the open interval $\boldsymbol{I}$, while the cross-sections are characterised by a unit normal vector field $\bar{\boldsymbol{n}}(S,t)$, as shown in the following:

$$S \in \boldsymbol{I} \rightarrow \varphi_0(S,t) \in \mathbb{R}^3, \quad S \in \boldsymbol{I} \rightarrow \bar{\boldsymbol{n}}(S,t) \in \mathbb{R}^3 \tag{1}$$

The motion of the beam model is based on the following assumptions: the cross-sections remain plane in the current (*spatial*) configuration (in other words, warping effects are not allowed) and the cross-sections do not

experience any change in shape or size. For simplicity, the model will be restricted to uniform cross-sections, and a straight line of centroids in the *reference configuration*. In order to express the equation of motion of the beam, it is often useful to introduce an *orthonormal frame* at each point of the curve $S \to \varphi_0(S,t)$ which will be referred to as *moving* or *intrinsic* frame: $\{\bar{\boldsymbol{t}}_1(S,t), \bar{\boldsymbol{t}}_2(S,t), \bar{\boldsymbol{n}}(S,t)\}$. Initially, any cross-section of the beam belongs to a plane normal to $\bar{\boldsymbol{E}}_3$. During the motion, the cross-sections exhibit a rigid body motion, which can be expressed in terms of an orthogonal transformation $S \to \underline{\boldsymbol{R}}(S,t) \in \mathrm{SO(3)}$[1] such that :

$$\bar{\boldsymbol{t}}_I(S,t) = \underline{\boldsymbol{R}}(S,t)\bar{\boldsymbol{E}}_I \tag{2}$$

where $\underline{\boldsymbol{R}}(S,t)$ maps the *reference frame* into the *moving frame*. In this context the *moving frame* is the *reference frame* rotated. Using the assumptions described previously, the deformation of the beam is characterised by the motion of the line of centroids and the rotation of the cross-sections, as illustrated in section 2.

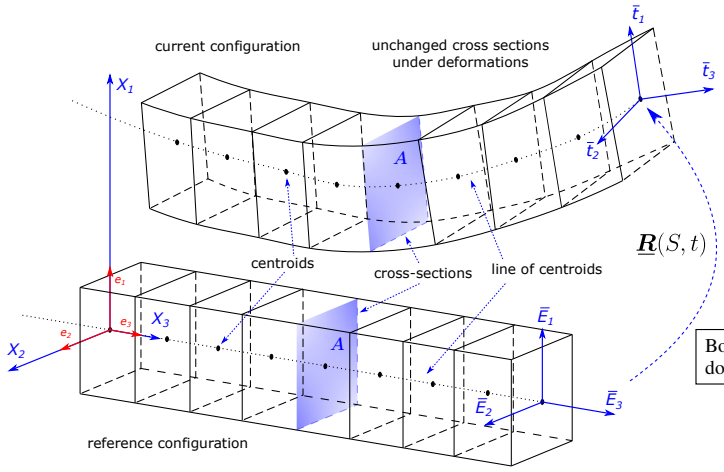

(a) Reference and current configurations in a three-dimensional representation; reference frame $\{\bar{\boldsymbol{E}}_1, \bar{\boldsymbol{E}}_2, \bar{\boldsymbol{E}}_3\}$; current frame $\{\bar{\boldsymbol{t}}_1, \bar{\boldsymbol{t}}_2, \bar{\boldsymbol{t}}_3\}$; set of coordinates $\{X_1, X_2, X_3\}$; global reference system $\{\bar{\boldsymbol{e}}_1, \bar{\boldsymbol{e}}_2, \bar{\boldsymbol{e}}_3\}$.

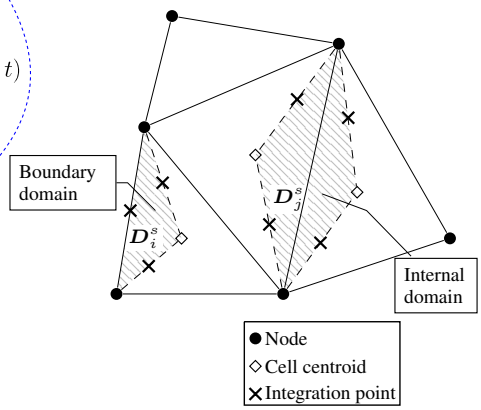

(b) Edge-based smoothing domains (2D case)

Figure 1

Although the original formulation of the model accounts for dynamic effects (see Simo [9]), in this paper, attention is devoted to the static case. One can demonstrate that the beam *spatial* stress measures, $\bar{\boldsymbol{f}}$ and $\bar{\boldsymbol{m}}$, must satisfy the following linear and angular momentum balance equations Simo [9]:

$$\frac{\partial \bar{\boldsymbol{f}}}{\partial S} + \bar{\boldsymbol{q}}_{\bar{\boldsymbol{f}}} = 0, \quad \frac{\partial \bar{\boldsymbol{m}}}{\partial S} + \frac{\partial \varphi_0}{\partial S} \times \bar{\boldsymbol{f}} + \bar{\boldsymbol{q}}_{\bar{\boldsymbol{m}}} = 0 \qquad S \in \boldsymbol{I} \tag{3}$$

where $\bar{\boldsymbol{q}}_{\bar{\boldsymbol{f}}}$ is the (applied) force per unit of reference arc length and $\bar{\boldsymbol{q}}_{\bar{\boldsymbol{m}}}$ is the (applied) moment per unit of reference arc length. It is often more convenient to use a *material* form of the beam model in applications. Material stress measures belong to the *reference configuration*, and can be obtained from the *spatial* measures through a *pull-back* operation, performed with the rotation tensor $\underline{\boldsymbol{R}}(S,t)$:

$$\bar{\boldsymbol{N}}(S,t) = \underline{\boldsymbol{R}}^T(S,t)\bar{\boldsymbol{f}}(S,t), \quad \bar{\boldsymbol{M}}(S,t) = \underline{\boldsymbol{R}}^T(S,t)\bar{\boldsymbol{m}}(S,t) \tag{4}$$

In this paper, aiming a simple approach, the adopted constitutive model is limited to the elastic case. However, this is not a limitation of the beam model, rather a simplification adopted in the context of this work. In addition

[1] This is the special orthogonal Lie group. See more in Geradin and Cardona [11].

to that, the material is assumed to be *homogeneous* and *isotropic*. For a particular case where the beam axis coincides with the cross-sectional centroids and the cross-sectional axis is parallel to the principal axis of inertia, the constitutive tensor $\underline{\boldsymbol{C}}$ is constant and diagonal. Therefore, the *material* version of the constitutive law can be represented by:

$$\left\{ \begin{array}{c} \bar{\boldsymbol{N}}(S,t) \\ \bar{\boldsymbol{M}}(S,t) \end{array} \right\} = \underline{\boldsymbol{C}} \left\{ \begin{array}{c} \bar{\boldsymbol{\Gamma}}(S,t) \\ \bar{\boldsymbol{\Omega}}(S,t) \end{array} \right\} \tag{5}$$

where $\bar{\boldsymbol{\Gamma}}(S,t)$ and $\bar{\boldsymbol{\Omega}}(S,t)$ are the *material* strain measures. The first one takes into account axial and shear deformations, while the second one takes into account bending and torsional deformations Simo [9], Geradin and Cardona [11]. These strain measures posses the following representation:

$$\bar{\boldsymbol{\Gamma}}(S,t) \equiv \underline{\boldsymbol{R}}^T \frac{\partial \varphi_0(S,t)}{\partial S} - \bar{\boldsymbol{E}}_3(S), \quad \bar{\boldsymbol{\Omega}}(S,t) \equiv \text{axial} \left[\underline{\boldsymbol{R}}^T(S,t) \frac{\partial \underline{\boldsymbol{R}}(S,t)}{\partial S} \right] \tag{6}$$

in equation above $\bar{\boldsymbol{\Omega}}(S,t)$ is the axial vector associated with the skew-symmetric tensor $\underline{\boldsymbol{\Omega}}(S,t)$ (see Simo and Vu-Quoc [10], Geradin and Cardona [11], Gori [14]).

3 Edge-based smoothed point interpolation method (ES-PIM)

In the smoothed point interpolation methods the concepts of smoothing domains and weakened-weak W^2 form are introduced. Such smoothing domains are used to transform the gradients of the field variables into boundary integrals using the Green's theorem (see Liu and Zhang [4]) for further details). In this work, each smoothing domain $\boldsymbol{D}_k^S$ is associated with an *edge* and its end points (nodes) coincide with the integration points used to perform the boundary integration over each smoothing domain.

3.1 Support nodes selection

In SPIMs a certain number of nodes is selected to compose the *support domain* S_d for each point of interest. In two-dimensions, the so-called T-schemes are usually employed for this task, where background triangular cells are used Liu and Zhang [4], as shown in Fig. 1b. In the present one-dimensional edge-based approach, the *edge*, background cells and smoothing domains occupy the same space as depicted in Fig. 2a. In order to evaluate the support nodes used to construct the shape functions at each integration point, two different strategies are proposed in this paper. With the so-called *L2-scheme*, the support domain at each integration point is constituted by the two nodes of the smoothing domain where the point belongs to (Fig. 2b). In the second approach, referred to as *L3/2-scheme*, for each integration point, the *support domain* is composed by the two nodes of the smoothing domain where the point belongs to, and an additional node from the neighbour smoothing domain, as illustrated in Fig. 2c. For integration points on the boundary of the model, the *L3/2-scheme* degenerates to the *L2-scheme*. In order to approximate the "field variables", it is necessary to compute the shape functions at the centre of the smoothing domains, in this case the support domain at the centre will be built as the *union* of the *left* and *right* supports of the same smoothing domain (see Fig. 2b and Fig. 2c).

3.2 Weakened-weak form

In SPIMs applications, the starting point to develop the weakened-weak formulation can be the weak form. Let us consider an arbitrary admissible variation related to displacements and rotations with the form $\bar{\boldsymbol{\eta}}(S,t) \equiv (\bar{\boldsymbol{\eta}}_0(S,t), \bar{\boldsymbol{\theta}}(S,t)) \in T_\varphi \mathcal{C}$ (see Simo and Vu-Quoc [10]). Starting from the linear and angular momentum balance equations shown in eq. (3), and using the admissible variations as test functions in a weighted residual procedure, a functional $G(\varphi, \bar{\boldsymbol{\eta}})$ can be introduced, in its *material* version [10]:

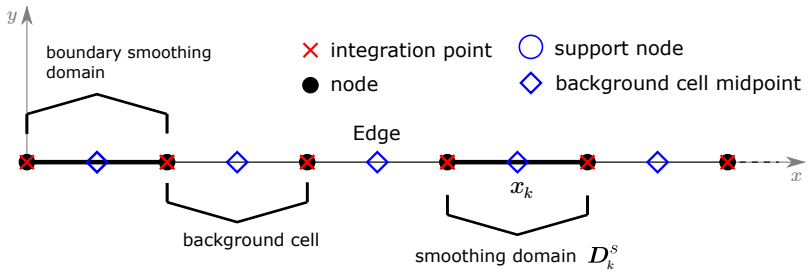

(a) Edge-based smoothing domains

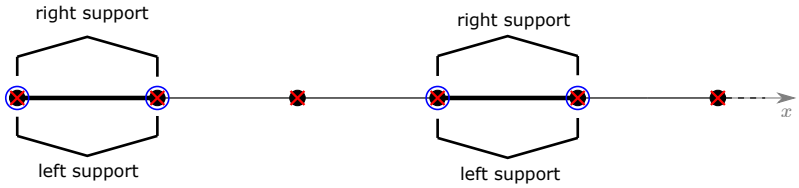

(b) L2-scheme

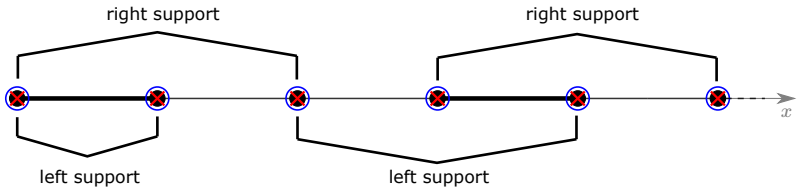

(c) L3/2-scheme

$$
\begin{aligned}
G(\varphi, \bar{\boldsymbol{\eta}}) \coloneqq & \int_{[0,L]} \left\{ \bar{\boldsymbol{N}} \cdot \underline{\boldsymbol{R}}^T \left[\frac{\partial \bar{\boldsymbol{\eta}}_0}{\partial S} - \bar{\boldsymbol{\theta}} \times \frac{\partial \varphi_0}{\partial S} \right] + \bar{\boldsymbol{M}} \cdot \underline{\boldsymbol{R}}^T \frac{\partial \bar{\boldsymbol{\theta}}}{\partial S} \right\} dS \\
& - \int_{[0,L]} (\bar{\boldsymbol{q}}_{\bar{\boldsymbol{f}}} \cdot \bar{\boldsymbol{\eta}}_0 + \bar{\boldsymbol{q}}_{\bar{\boldsymbol{m}}} \cdot \bar{\boldsymbol{\theta}}) \, dS
\end{aligned}
\tag{7}
$$

The weak form of the beam problem consists then into find a configuration such that $G = 0, \forall \bar{\boldsymbol{\eta}} \in T_\varphi \mathcal{C}$. In order to obtain a solution algorithm for the geometrically nonlinear beam problem, the weak form must be linearised. The linearisation procedure of the functional $G(\varphi, \bar{\boldsymbol{\eta}})$ is achieved by considering its tangent approximation at the configuration $\varphi = \hat{\varphi}$ (see Wriggers [12, p. 96]) as follows[2]:

$$
L[G(\hat{\varphi}, \bar{\boldsymbol{\eta}})] = G(\hat{\varphi}, \bar{\boldsymbol{\eta}}) + DG(\hat{\varphi}, \bar{\boldsymbol{\eta}}) \cdot \Delta\varphi \tag{8}
$$

For a detailed explanation regarding the linearisation procedure the reader is referred to Simo and Vu-Quoc [10], Geradin and Cardona [11], Gori [14]. With above equation, it is possible to move towards a suitable numerical method that makes use of a weak form, for instance, the finite element method. In SPIMs applications the weakened-weak form is obtained by considering that the strain measures, $\bar{\boldsymbol{\Gamma}}(S,t)$ and $\bar{\boldsymbol{\Omega}}(S,t)$, are *constants* within each smoothing domain $\boldsymbol{D}_k^S$. This is achieved by replacing the strain measures of each smoothing domain by their smoothed versions (see Liu and Zhang [4]). In the current beam model, the strain measures $\bar{\boldsymbol{\Gamma}}(S,t)$ and $\bar{\boldsymbol{\Omega}}(S,t)$ are replaced by $\widetilde{\bar{\boldsymbol{\Gamma}}}(x_k)$ and $\widetilde{\bar{\boldsymbol{\Omega}}}(x_k)$, as shown in the following:

$$
\widetilde{\bar{\boldsymbol{\Gamma}}}(x_k) = \frac{\underline{\boldsymbol{R}}^T(x_k)}{\ell_k} \left[\varphi_0(\xi) \, n_S^{(k)}(\xi) \right] \Big|_{\boldsymbol{\Gamma}_k} - E_3(S), \quad \widetilde{\bar{\boldsymbol{\Omega}}}(x_k) = \text{axial} \left[\frac{\underline{\boldsymbol{R}}^T(x_k)}{\ell_k} \left[\underline{\boldsymbol{R}}(\xi) \, n_S^{(k)}(\xi) \right] \Big|_{\boldsymbol{\Gamma}_k} \right] \tag{9}
$$

[2]For a broader and more formal overview regarded to the linearisation procedure, see Marsden and Hughes [13].

with $\widetilde{\widetilde{\mathbf{\Omega}}}(x_k) = \text{axial}[\widetilde{\underline{\mathbf{\Omega}}}(x_k)]$, where x_k is the centre of the smoothing domain k, n_S^k represents the normal outward unit vector, however it takes $+1$ or -1 in the one-dimensional case, $\mathbf{\Gamma}_k$ represents the smoothing domain boundary, and ℓ_k is the smoothing domain length. After performing the smoothing operation above, the domain integrals appearing in eq. (8) (see Simo and Vu-Quoc [10]) can be transformed in a summation over the N_S smoothing domains composing the discrete model, resulting in the following weakened-weak form:

$$\widetilde{L}[G(\varphi, \bar{\boldsymbol{\eta}})] = \widetilde{G}(\hat{\varphi}, \bar{\boldsymbol{\eta}}) + \widetilde{DG}(\hat{\varphi}, \bar{\boldsymbol{\eta}}) \cdot \Delta\varphi \tag{10}$$

4 Numerical simulations

In what follows, the numerical results of a classic example are illustrated for the L2 and L3/2 schemes. The linear FEM with a *reduced integration* was also simulated, however, the obtained results were identical to the L2-scheme results, therefore they were omitted. The simulations were performed by a Newton-like algorithm with load control. The present example is a right-angle hinged frame[3] subjected to a *fixed* load or a *follower* load. The same input data presented in Simo and Vu-Quoc [10] are adopted in this work. Each component of the frame is discretised with 5 smoothing domains.

Problem data: the frame is characterised by each component having $L = 120\,\text{mm}$ with a point load placed at the distance $a = (1/5)L$, as shown in Figure 3. The following geometric and material information were adopted in the simulations:

$$\begin{array}{llll} A = 6\,\text{mm}^2 & I_1 = 2\,\text{mm}^4 & & \\ A_1 = 6\,\text{mm}^2 & I_2 = 2\,\text{mm}^4 & E = 7\,200\,000\,\text{N/mm}^2 & \\ A_2 = 6\,\text{mm}^2 & J_t = 4\,\text{mm}^4 & G = 2\,770\,000\,\text{N/mm}^2 & \end{array} \tag{11}$$

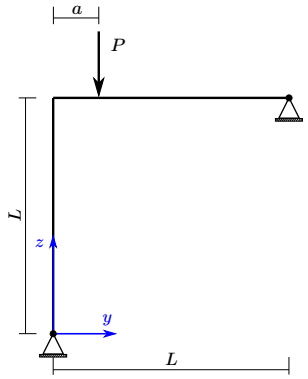

Figure 3. Hinged right-angle frame under a force load

During the simulations, the load was incremented until the frame reached the buckling load. The L2 and L3/2 schemes were analysed with a *fixed* and a *follower* load starting from the same magnitude $P = 1000\,\text{N}$. The deformed shapes due to the *fixed* load are shown in Fig. 4a and Fig. 4b, while in Fig. 4c and Fig. 4d the deformation due to the *follower* load case are illustrated. With respect to the buckling load, the L2 and L3/2 schemes exhibited a similar outcome, as can be observe in Fig. 4e and Fig. 4f, while in Table 1 the estimated values for the buckling load are illustrated. The analytical solution of the buckling load for a *fixed* load is available in Lee et al. [15]. Considering an elastic frame, the expected value of the buckling load is $P = 18.552(EI/L^2) = 18\,552\,\text{N}$. The results presented in Table 1 agree with this value, as the errors of L2 and L3/2 schemes are inferior to 6% when compared with the expected solution.

[3]Some authors refer it as the Lee's frame, due to the work of Lee et al. [15] where this frame was first studied and analytical solutions provided.

The L3/2 results showed a *softer* behaviour than the L2-scheme. In other words, the buckling load achieved for the L2-scheme simulation is bigger than the L3/2-scheme outcome. Performing the same simulations with the linear FEM, the same results obtained for the L2-scheme are recovered for both load types.

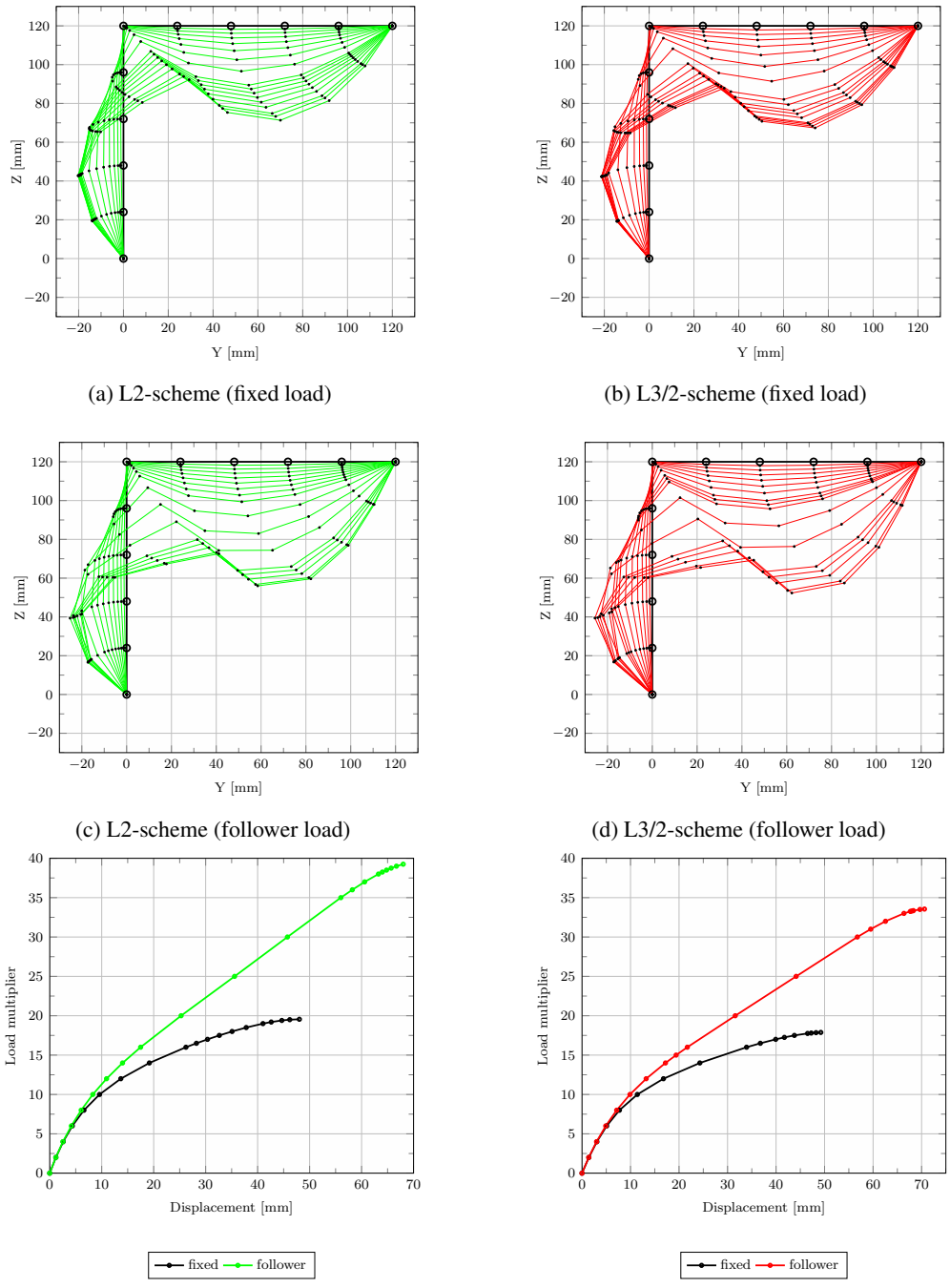

(a) L2-scheme (fixed load)

(b) L3/2-scheme (fixed load)

(c) L2-scheme (follower load)

(d) L3/2-scheme (follower load)

(e) L2-scheme (load-displacement diagram)

(f) L3/2-scheme (load-displacement diagram)

Figure 4. Numerical results

Table 1. Load buckling values in Newtons

Load	L2 scheme	Simo (1986)	Δ [%]	L3/2 Scheme	Simo (1986)	Δ [%]
fixed	19550	18532	5.49	17880	18532	-3.52
follower	39250	35447	10.73	33580	35447	-5.27

5 Conclusions

This paper presented a preliminary investigation on the application of SPIM meshfree models to the analysis of a geometrically exact beam. The numerical simulations pointed out that depending on the number of *support nodes* used to construct the shape functions, different behaviours were identified. Using the L2-scheme, the same solution of the linear FEM with *reduced integration* was recovered, while using the L3/2-scheme a *softer* solution was obtained. This same behaviour was observed in Santos et al. [8] referring to the *lower* and *upper* bound solutions of the linear Timoshenko beam. Moreover, different from FEM implementations, the proposed meshfree approach does not require a numerical integration along the beam, neither to evaluate the jacobian necessary in isoparametric FEM formulations. Finally, the proposed SPIMs exhibited a locking free behaviour, i.e. no additional treatment was necessary to avoid the *spurious stiffer behaviour* that commonly occurs in FEM simulations of shear-deformable beams.

Acknowledgements. The first and third authors gratefully acknowledge the financial support of the CNPq (in portuguese: Conselho Nacional de Desenvolvimento Científico e Tecnológico).

Authorship statement. The authors hereby confirm that they are the sole liable persons responsible for the authorship of this work, and that all material that has been herein included as part of the present paper is either the property (and authorship) of the authors, or has the permission of the owners to be included here.

References

[1] G. Liu, G. Zhang, K. Dai, Y. Wang, Z. Zhong, G. Li, and X. Han. A linearly conforming point interpolation method (lc-pim) for 2d solid mechanics problems. *International Journal of Computational Methods*, vol. 2, n. 04, pp. 645–665, 2005.

[2] G. Zhang and G.-R. Liu. A meshfree cell-based smoothed point interpolation method for solid mechanics problems. In *AIP Conference Proceedings*, volume 1233, pp. 887–892. American Institute of Physics, 2010.

[3] G. Liu and G. Zhang. Edge-based smoothed point interpolation methods. *International Journal of Computational Methods*, vol. 5, n. 04, pp. 621–646, 2008.

[4] G.-R. Liu and G.-y. Zhang. *Smoothed point interpolation methods: G space theory and weakened weak forms*. World Scientific, 2013.

[5] G.-R. Liu. A generalized gradient smoothing technique and the smoothed bilinear form for galerkin formulation of a wide class of computational methods. *International Journal of Computational Methods*, vol. 5, n. 02, pp. 199–236, 2008.

[6] C. Du, D. Zhang, L. Li, and G. Liu. A node-based smoothed point interpolation method for dynamic analysis of rotating flexible beams. *Acta Mechanica Sinica*, vol. 34, n. 2, pp. 409–420, 2018.

[7] C. He, X. Wu, T. Wang, and H. He. Geometrically nonlinear analysis for elastic beam using point interpolation meshless method. *Shock and Vibration*, vol. 2019, 2019.

[8] F. P. Santos, E. Marino, and L. Gori. A meshfree approach for the timoshenko beam. In *XLII Ibero-Latin-American Congress on Computational Methods in Engineering (CILAMCE-2021)*, 2021.

[9] J. Simo. A finite strain beam formulation. the three-dimensional dynamic problem. part i. *Computer Methods in Applied Mechanics and Engineering*, vol. 49, n. 1, pp. 55–70, 1985.

[10] J. Simo and L. Vu-Quoc. A three-dimensional finite-strain rod model. Part II: Computational Aspects. *Computer Methods in Applied Mechanics and Engineering*, 1986.

[11] M. Geradin and A. Cardona. A beam finite element non-linear theory with finite rotations. *International Journal for Numerical Methods in Engineering*, vol. 26, 1988.

[12] P. Wriggers. *Nonlinear finite element methods*. Springer Science & Business Media, 2008.

[13] J. E. Marsden and T. J. Hughes. *Mathematical foundations of elasticity*. Courier Corporation, 1994.

[14] L. Gori. Geometrically exact three-dimensional beam theory: Fem implementation and applications. Master's thesis, Universitá degli Studi di Firenze, 2014.

[15] S.-L. Lee, F. S. Manuel, and E. C. Rossow. Large deflections and stability of elastic frames. *Journal of the Engineering Mechanics Division*, vol. 94, n. 2, pp. 521–548, 1968.